Experimental characterisation and modelling of breast Cooper's ligaments

N. Briot, G. Chagnon, L. Burlet, H. Gil, E. Girard, Yohan Payan

Experimental characterisation and modelling of breast Cooper's ligaments

N. Briot*[1], G. Chagnon[1], L. Burlet[3], H. Gil[4], E. Girard[2,3], and Y. Payan[1]

[1]Univ. Grenoble Alpes, CNRS, UMR 5525, VetAgro Sup, Grenoble INP, TIMC, 38000 Grenoble, France
[2]Univ. Grenoble Alpes, CNRS, UMR 5525, VetAgro Sup, Grenoble INP, CHU Grenoble Alpes, TIMC, 38000 Grenoble, France
[3]Laboratoire d'Anatomie des Alpes Française, Faculté de Médecine, Domaine de la Merci, F-38700 La Tronche Cedex
[4]Département d'anatomopathologie et cytologie, Centre Hospitalier Grenoble-Alpes, 38000 Grenoble, France

* Corresponding author : noemie.briot@univ-grenoble-alpes.fr

Abstract

The aim of this study was to characterise the mechanical behaviour of Cooper's ligaments. Such ligaments are collagenous breast tissue that create a three-dimensional structure over the entire breast volume. Ten ligaments were extracted from a human cadaver, from which 28 samples were cut and used to perform uniaxial tensile tests.

Histological analysis showed that the main direction of the fibres visible to the naked eye corresponds to the orientation of the fibres on a microscopic scale. The specimens were cut according to this orientation, which allowed the sample to be stretched in the main fibre direction. From these experimental stretch/stress curves, an original anisotropic hyperelastic constitutive law is proposed to model the behaviour of Cooper's ligaments and the material parameter validity is discussed.

1 Introduction

Numerous studies propose biomechanical modelling of human breast tissues with different goals such as the localisation of breast tumours during surgery (Del Palomar et al., 2008; Samani et al., 2007), the prediction of breast behaviour after the implantation of a prosthesis (Lapuebla-Ferri et al., 2011), surgical training for biopsy (Azar et al., 2001) or computer assisted medical interventions (Carter, 2009; Han et al., 2011; Ruiter et al., 2006). Most studies use Finite Element (FE) modelling. The expected results are numerous and various, such as the prediction of the shape of the breast, the pain experienced by a patient during a mammogram (Chung et al., 2008), or the deformation of tissue due to a biopsy needle (Azar et al., 2000).

Different approaches of modelling are provided in the literature. Samani et al. (2001) proposed to use a global model of the breast that did not include the various constituents of breast

tissues such as skin, muscles, ligaments, fascia, fat or glandular tissue. Mîra et al. (2018) high-lighted in FE simulations the importance of suspensory ligaments as well as superficial and deep fasciae. The models proposed by Azar et al. (2000, 2001) tried to consider the mechanical influence of the Cooper's ligaments by using a global parameter to represent both fat and ligaments or glandular tissue and ligaments.

All these FE simulations face difficulties in estimating the mechanical properties of each constituent of breast tissue. If some constitutive laws were proposed in the literature to model skin, muscle and fat tissues, very little data is available concerning breast ligaments and fasciae.

Among all the structures of the breast, the suspensory ligaments, and in particular the Cooper ligaments, have a specific role. These ligaments form a kind of 3D mesh, which includes fat lobules and mammary lobules. To our knowledge, there is no FE model that includes the Cooper's ligaments as such or uses the intrinsic mechanical properties of these ligaments. This may be due to the fact that no experimental data is available to estimate the mechanical properties of these ligaments.

In a preliminary study presented during the 25th Conference of the French Biomechanical Society (Briot et al., 2020), an *ex vivo* experiment of the mechanical behaviour of Cooper's ligaments under uniaxial tensile test was performed (based on a cadaver dissection) in order to propose a constitutive model for these ligaments. This paper aims at completing this preliminary study, with a detailed analysis of the 28 uniaxial tensile tests and with the proposal of an original anisotropic hyperelastic constitutive law to model the mechanical behaviour of Cooper's ligaments.

In the following, the 'Material and Methods' section introduces Cooper's ligaments and describes the uniaxial tensile tests. These tests are then analysed in the 'Results and discussion' section, with the proposal of an original anisotropic, hyperelastic constitutive law. The paper ends with a conclusion and some perspectives.

2 Material and Methods

Firstly, details are given about the anatomy of the breast while secondly, the preparation of the specimens and the mechanical tests are described.

2.1 Cooper's ligaments

2.1.1 Anatomical description of the breast

The breast is a passive organ presenting a complex structure (Gaskin et al., 2020). Breast anatomy can be described as a set of layers of various tissues as presented in Figure 1. The organ originates in its upper part at the level of the clavicle and ends in its lower part at the level of the sixth rib. Laterally, the breast is located between the sternum and the lateral part of the rib cage starting from the axillary hollow.

From a superficial point of view, the breast is covered with skin, like the whole body. This skin is mainly composed of three layers: the epidermis, the dermis and the hypodermis. In the centre of the skin's superficial layer is the nipple surrounded by the areola. Internally, the entire breast rests on the pectoralis muscles, which are attached to the ribs.

Right in the middle of the breast volume is the mammary gland. This gland is made up of lobules which are themselves responsible for the production of milk. These mammary lobules group together to form the galactophoric ducts which join the nipple to convey the milk. The mammary gland is itself surrounded by adipose tissue that forms the main volume of the breast.
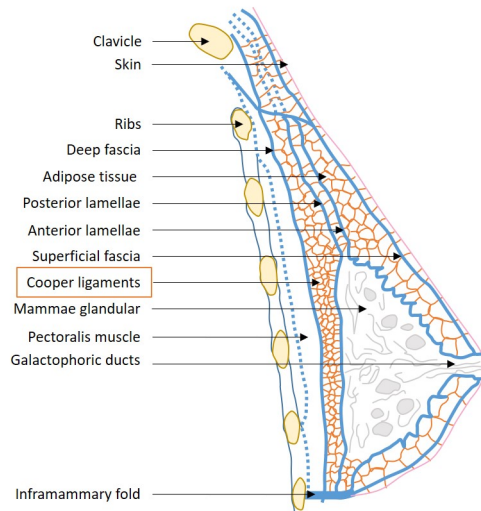
Figure 1: Breast anatomical description

There are several conjunctive tissues composed of collagen throughout the entire breast volume. The first type of collagenous tissue is fascia: the deep fascia located between the pectoral muscles and the breast volume (gland + adipose tissue) and the superficial fascia located between the skin and the breast volume. The second type of collagenous tissue are the posterior and anterior lamellae that encompass the entire mammary gland. These two types of collagenous tissue (fascia and lamellae) meet at the level of the clavicle and at the level of the inframammary fold (located at the lower limit of the breast). The third type of collagenous tissue are Cooper's ligaments. Their anatomical description varies from one article to another. Gefen and Dilmoney (2007) describe Cooper's ligaments as the tentacles extending from the mammary gland while Gaskin et al. (2020) describe them as a three-dimensional mesh forming pockets of adipose tissue. This description of Cooper's ligaments from Gaskin et al. (2020) is adopted here since it corresponds to what was observed during our experimental dissections as illustrated in Figure 2.
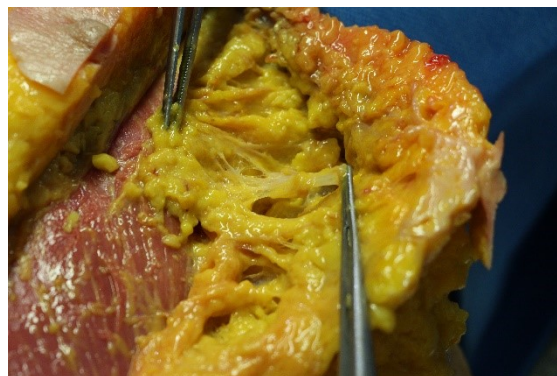

Figure 2: Dissection picture of the three-dimensional mesh of Cooper's ligaments forming pockets of adipose tissue

3

2.1.2 Sample extraction

In accordance with French regulations on postmortem testing, a breast anatomical dissection was performed at the Anatomy Laboratory, Grenoble Faculty of Medicine, on a female cadaver (100 years old, 164 cm tall and 70 kg). Because of the COVID-19 pandemic situation, fresh cadavers were not available for dissection. The cadaver was embalmed using a formalin solution, injected in the carotid artery and drained from the jugular vein and then preserved in a refrigerated room. The dissection occurred 12 days after the death.

To access Cooper's ligaments the following dissection technique was used. A lateral incision was made, subclavicular then medioaxillary, to expose the chest wall and lay the breast inside out on the sternum. The posterior part of the breast was thus exposed, which facilitates the extraction of the cooperating ligaments. Dissection of the breast was then performed from the posterior to the anterior plane. The corresponding cutting diagram is shown in Figure 3. The advantage of this method is that it provides clear anatomical landmarks (the pectoralis muscles are easily identifiable), which allows to better discern and locate the samples. Ten extractions (from the two breasts of our single corpse) were carried out, from which 28 samples were cut.

As illustrated in Figure 2, Cooper's ligaments form a 3D mesh structure that creates pockets containing adipose tissue. This adipose tissue had to be removed to extract the Cooper's ligaments.
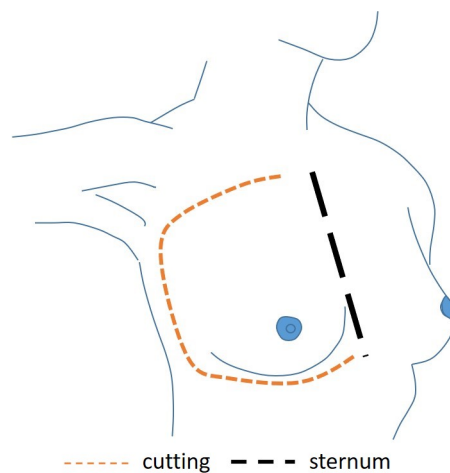
Figure 3: Dissection method

2.1.3 Histological analysis

By eye, the ligament gives the impression of having a structure with unidirectional fibres that are aligned in the direction of the ligament. To confirm this visual inspection and to analyse the tissue in detail, a histological analysis was performed.

Samples were conserved in formaldehyde, fixed first in formalin 10% for 24 hours at 4°C and then embedded in parafin according to the usual protocol (Canene-Adams, 2013). Sections of 3 µm were then realised with a microtome Leica RM 2245 (Wetzlar, Germany). The slices were then stained with Hematoxylin Eosin Saffron (HES) to see nucleic acids and connective tissue (amongst other collagen), or with Orcein staining to highlight elastin fibres. Slices were then examined qualitatively by light microscopy focusing particularly on the elastin and collagen fibres' orientation. Pictures were acquired by a digital camera (Leica Microsystems) connected to an optical microscope (Leica Microsystems) and are presented in Figure 4.

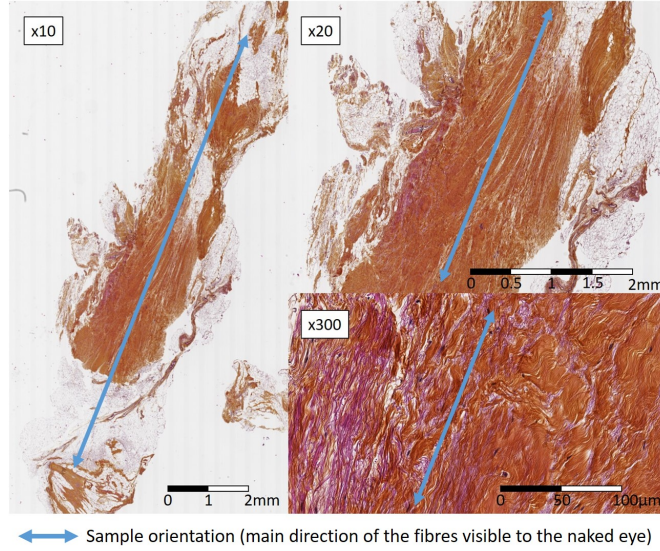Figure 4: Histology scan of a longitudinal section of a Cooper's ligament-HES (hematoxylin eosin saffron)-zoom x10, x20 and x300

Elastin and collagen fibres have a predominant orientation in the longitudinal direction of the Cooper's ligament which corresponds to the direction visible to the naked eye. With the HES staining technique, elastin fibres appear purple on the histological scan and collagen fibres appear golden yellow.

The images confirm that the tissue fibres are oriented in one main direction. The material can thus be considered as a unidirectional composite material with the direction of reinforcement corresponding to the main direction of the ligament.

2.2 Description of uniaxial tensile tests

The histological study showed that the material has a fibrous direction. So, in principle, tests along two directions are needed to perfectly characterize the tissue, namely the fibre direction and the orthogonal one. Nevertheless, given the geometry of the ligaments (Figure 2), it was not possible to cut specimens along the orthogonal direction; so the study was limited to uniaxial tensile tests in the direction of the fibres.

The tensile tests were carried out using a MTS machine model C42 503, equipped with a +/-25N load cell. This tensile machine was equipped with a watertight tank (Masri et al., 2017). To get as close as possible to the physiological conditions of stress, the tank was filled with a physiological saline maintained at a temperature of 37°C. Each uniaxial tensile test was carried out in the watertight tank by using immersed grips, an illustration at which is presented in Figure 5. These grips have the specific feature of being able to prevent the samples from slipping. The tests were conducted at a speed of 1%/s. A small pre-load in the range of 0.1N was applied to the samples to ensure their initial shape and avoid possible buckling.

The force and displacements were measured for each test, allowing for the evaluation of the stretch and the stress in the ligament. The uniaxial Cauchy stress is defined by:

$$\sigma = \frac{F}{A} \tag{1}$$

where F is the force applied to the sample and A the current cross-section area of the sample (evaluated from the initial section with the incompressibility hypothesis). The stretch is defined
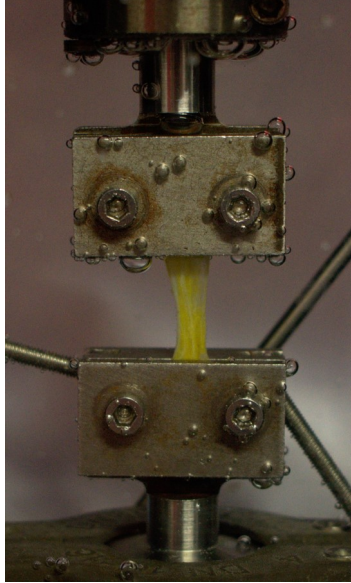
Figure 5: Cooper's ligament sample in grips without the watertight tank for photography needs

by:

$$\lambda = \frac{l}{L_0} \tag{2}$$

where l is the current grip-to-grip length of the sample and L_0 is the initial grip to grip length of the sample.

3   Results and discussion

3.1   Specimen analysis

The geometry of Cooper's ligaments is different depending on their location in the breast, and their width and thickness can vary significantly. This explains why samples of different shapes were extracted from the dissection: sample lengths vary between 13.9 mm and 15.1 mm, while their widthes and thicknesses were measured between 1.4 mm and 4.9 mm and between 0.04 mm and 0.3 mm, respectively.

Normally, a tensile test requires that the sample height/width ratio is sufficient to remain within the uniaxial reaction assumptions. Figure 6 shows the distribution of this ratio for all 28 specimens. Specimens with a ratio of less than 5 are supposed to be under the limit of the uniaxial stress assumptions. But it should be remembered that the shape and size of the specimens are mainly related to the morphological conditions and to the location where the samples were taken.

Cooper's ligament samples have a fluctuating proportion of fat which strongly influences the thickness of the samples. Although the outer fat was removed as carefully as possible, it was very difficult and sometimes impossible to remove the central fat from the thicker specimens. Thus, when the samples were the thickest, this meant that adipose tissue could be present in the specimen. Conversely, when the specimens were thinner, this encouraged the appearance of holes in the specimen. In both cases, this could distort the homogeneity.

Because of this high variability in terms of sample thickness, it was decided to define three groups gathering (1) the 'too thin' samples with thicknesses below 0.063 mm, (2) the 'too thick'
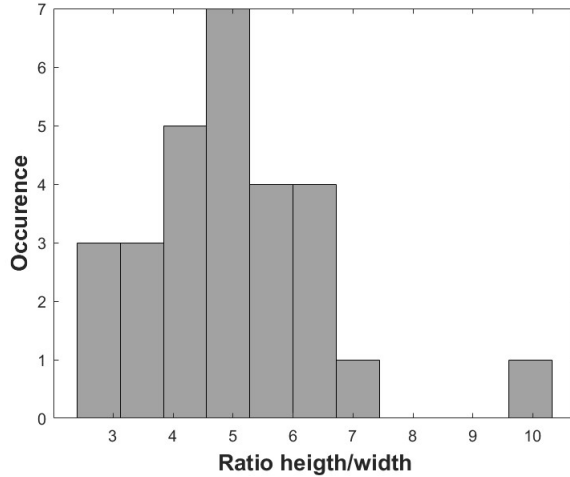
Figure 6: Histogram of height to width ratio for the different specimens

samples with thicknesses above 0.21 mm and (3) the other samples with thicknesses that range between 0.063 and 0.21 mm which correspond to a standard deviation thickness around the average value.

3.2 Experimental results

A typical stress/stretch curve is presented in Figure 7. The beginning of the curve ($\lambda < 1.01$) has a relatively low slope and then presents a hardening until tearing starts to occur ($\lambda = 1.045$). The curve then presents different angular points corresponding to the progressive rupture of the ligament. Several breaks can be observed before the measured stress starts to decrease. In this study, the beginning of the tearing is assumed as the rupture of the specimen. Therefore, only the first part of the curve, the black dotted line, in Figure 7, is considered here. In the remaining paper, the curves will be only presented until the first crack apparition. This will be considered as the rupture point.

The 28 performed uniaxial tensile tests were divided into five groups according to the criteria (height/width ratios and thicknesses) discussed in the previous Section (Section 3.1):

- Group 1: all tests with a height/width ratio of less than 5

- Group 2: all tests with a height/width ratio higher than 5

- Group 3: all tests with a thickness of less than 0.063mm

- Group 4: all tests with a thickness ranging between 0.063 and 0.21mm

- Group 5: all tests with a thickness higher than 0.21mm

Two other subdivisions of the tests were also proposed:

- Standard (Stand): which includes tests that satisfy the normative criteria (ratio>5 and 0.063mm<thickness<0.21mm).

- Non-standard (NStand): all tests that do not respect the classical standard in terms of ratio and thickness.
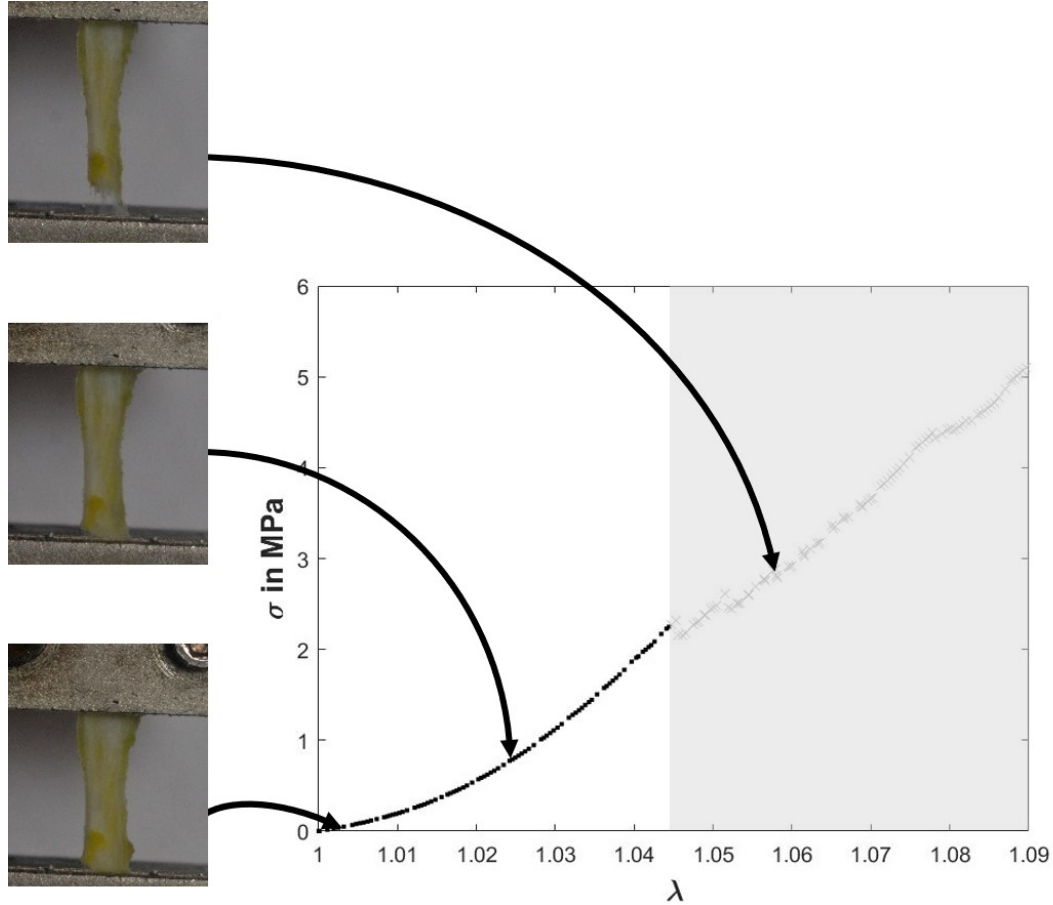
7

Figure 7: Typical stress/stretch curve of a Cooper's ligament uniaxial tensile test

These two subdivisions are plotted in Figure 8, thus summarizing the 28 performed uniaxial tensile tests (each presented until the first break). It is to note that a wide dispersion in the results can be observed despite the samples coming from the same person. However, the overall shape of the curves between the starting point and the first tissue break is similar for all the tests. The curves follow a highly non-linear form, which is classical for human soft tissues.

The first rupture point of each curve is measured and the results are summarised in Table 1.

3.3 Modelling

The ligaments have a clear non-linear elastic behaviour. It is assumed, in a first approximation, to represent them with a hyperelastic constitutive equation. If the ligaments would have been considered as one-dimension structures, an isotropic constitutive law could have been adopted (Briot et al., 2020). The method was effective in describing the stress-strain curve in the fibre direction but it is clear that the response in the orthogonal direction is not representative. However, following our histological observations (Figure 4), such Cooper's ligaments present a clear composition of fibres and extracellular matrix. Therefore, even if only one loading direction has been tested, it is decided to use an anisotropic constitutive equation. There exist many constitutive equations (and the corresponding strain energy density W) for such anisotropic materials (Chagnon et al., 2015). Most equations are composed of two parts, one isotropic part representing the matrix (W_{matrix}) and an anisotropic part representing the fibres (W_{fibres}) so that $W = W_{matrix} + W_{fibres}$. This approach will be used here. Due to the limitation of loading cases (it is impossible to perform biaxial or planar tensions test on Cooper's ligaments), it is
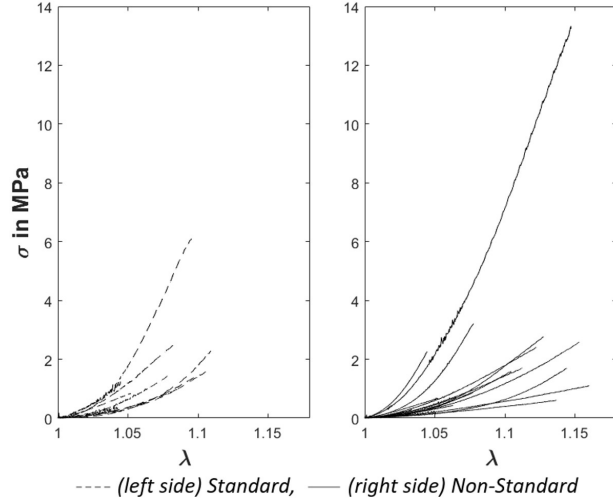
Figure 8: Results of uniaxial tensile tests for all the Cooper's ligament samples

Group	Nb of tests in a group	Average	Min	Max	Stand. Dev.
		Rupture Stretch in %			
1	16	7.7	3.0	15	3.6
2	12	9.8	3.4	16	4.0
3	3	7.8	4.3	15	6.0
4	20	9.1	3.0	16	3.9
5	5	8.5	3.4	13	3.4
Stand	8	7.4	3.0	11	3.0
NStand	20	9.1	3.4	16	4.1
All tests	28	8.9	3.0	76	3.9
		First Rupture Stress in MPa			
1	16	2.6	0.24	13	3.7
2	12	1.5	0.28	3.2	0.92
3	3	4.9	0.33	13	7.2
4	20	1.7	0.24	6.1	1.3
5	5	1.3	0.28	2.8	0.92
Stand	8	1.9	0.24	6.1	1.9
NStand	20	1.4	0.28	3.2	0.88
All tests	28	2.0	0.24	13	2.5

Table 1: First rupture values estimated from the 28 experimental tests

decided to focus on representative constitutive equations with a limited number of parameters to avoid non-physical fitting.

The isotropic part of the model is assumed as:

- Neo-Hookean modelling (Treloar, 1943):

$$W_{matrix} = C_1(I_1 - 3) \tag{3}$$

For the anisotropic part, two models of the literature with a limited number of parameters will be evaluated, namely a polynomial form and an exponential one:

- Triantafyllidis and Abeyaratne (1983) modelling:

$$W_{fibres} = C_2(I_4 - 1)^2 \tag{4}$$

- Holzapfel et al. (2000) modelling:

$$W_{fibres} = \frac{k_1}{2k_2}\left(e^{k_2(I_4-1)^2} - 1\right) \tag{5}$$

Where C_1, C_2, k_1 and k_2 are material parameters, I_1 represents the first invariant of the right Cauchy Green strain tensor $\overline{\overline{C}}$ and I_4 the fourth invariant defined by trace $(\overline{\overline{C}} \cdot \overrightarrow{a_0} \otimes \overrightarrow{a_0})$, where $\overrightarrow{a_0}$ is the initial orientation of the fibres in the ligament (in our case it corresponds to the tensile direction). The uniaxial Cauchy stress, projected along the stress axis, is defined in the incompressible framework for each model by:

$$\sigma = 2\left(\lambda^2 - \frac{1}{\lambda}\right)\frac{\partial W}{\partial I_1} + 2\lambda^2 \frac{\partial W}{\partial I_4} \tag{6}$$

The Triantafyllidis and Abeyaratne model has two parameters. The first parameter is related to the Neo-Hookean model which models the behaviour of the extracellular matrix, C_1. The second parameter is linked to the behaviour of the fibres, C_2. The Holzapfel model also has the C_1 parameter for the matrix but has two other parameters k_1 and k_2 for the fibres' behaviour.

Each experimental curve is fitted independently for the 28 tests. The results of the material parameter optimization are presented in Table 2. In this table, for each model, the calculated error is the average of the point-by-point errors in the least squares sense. It appears that for both models C_1 was obtained null in 28 cases out of 28. This would mean that the contribution of the extracellular matrix (Laurent, 2018) is zero although it is present in the material. This underlines that the results of a global identification disagree with the experimental observations. This result is due to the fact that the two equations of both models link the material parameters to describe the initial slope of the material. This initial slope can be approximated by a linearisation of equation 6 where we get what some might call the Young's modulus E of the material.

- Triantafyllidis modelling:

$$E = 6C_1 + 8C_2 \tag{7}$$

- Holzapfel modelling:

$$E = 6C_1 + 4k_1 \tag{8}$$

The limits of both modelling are reached here with a small number of test conditions and a global identification of the behaviour of the material. To overcome this problem, it is proposed to introduce a hyperelastic strain energy density where the fibre parameters are only involved in large strain. The objective is to fit the isotropic and anisotropic parameters in different strain zones in order to ensure the uniqueness of the material parameters. It is often considered in literature that the tissue should endure some percents of deformation before being stretched. Jemioło and Telega (2001) proposed a series development depending of four invariants, isotropic and anisotropic ones:

$$W_{jemiolo} = \sum_{klmn} c_{klmn}(I_1 - 3)^{a_k}(I_2 - 3)^{b_l}(I_4 - 3)^{c_m}(I_5 - 3)^{d_n} \tag{9}$$

In a first approach it is decided to limit the number of parameters and keep only two terms:

$$W_{fibres} = C_1(I_1 - 3) + b_1(I_4 - 1)^{b_2} \tag{10}$$

b_1 and b_2 being material parameters describing the strain hardening. The initial slope is calculated by a linearisation of the strain/stress curve, all the details are given in the appendix:

$$E = 6C_1 \tag{11}$$

If $b_2 = 2$, the initial slope is given by:

$$E = 6C_1 + 8b_1 \tag{12}$$

In the first case, the slope is only depending on the isotropic parameter which is what is required. In the other case ($b_2 = 2$), E is not only dependent on C_1, but finding b_2 strictly equal to 2 is very rare and nearly impossible in a fitting procedure. As a consequence, the fitting process can be decomposed into two steps, C_1 is first fitted at the beginning of the experimental stretch/stress curves and the two other parameters b_1 and b_2 are fitted to describe the rest of the curves.

The values of the parameters estimated for each test are presented in Table 2. First, to note, no C_1 parameter was fitted to 0. As an example, for test N°5, Figure 9 superimposes the analytical stretch/stress curves computed for all the three models. Those three models were run for all samples. Error bars plotted in this figure correspond to uncertainties in the measurements due to uncertainties in the estimation of the ligament section (width and thickness). If one looks at the curves globally, the three models seem to give results that are consistent with the experimental errors. However, if one zooms in on the initial part of the curve, it can be observed that the power law model is the only one which is able to correctly describe the initial slope. Out of all 28 tests, the Triantafyllidis modelling is within the model validity area (represented by the error bars) in 36% of the cases. The Holzapfel modelling is within the model's area of validity in 57% of the cases. The power modelling is within the validity range of the model in 93% of the cases.

Since all samples come from the same body, the effects of dispersion do not involve variations from one individual to another. Dispersion can therefore only be explained by the fact that the samples are different and because of classical experimental errors and errors arising from difficulties in characterising biological tissue.

Considering the non-linearity of the results obtained, two parameters are interesting to deal with: the slope at the origin and the stiffening (slope at a strain of 5%). The experimental results present a non neglectible dispersion, the standard deviation is 5 MPa for Young's modulus and 20MPa for tangent modulus.

Further to this, a study of the dispersion of the Young's modulus was carried out in order to deduce the range of variation of the Young's modulus of the Cooper's ligaments.

Table 3 shows for each test the Young's modulus deduced from the C_1 parameter of the new model with the following law:

$$E = 6C_1 \tag{13}$$

Figure 10 shows the overall distribution of the Young's moduli obtained. A distribution law can then be set up to best represent the distribution established.

Frechet's law was chosen for such a distribution because it is generally used to represent the frequency of occurrence of singular phenomena. Its distribution law is defined as follows:
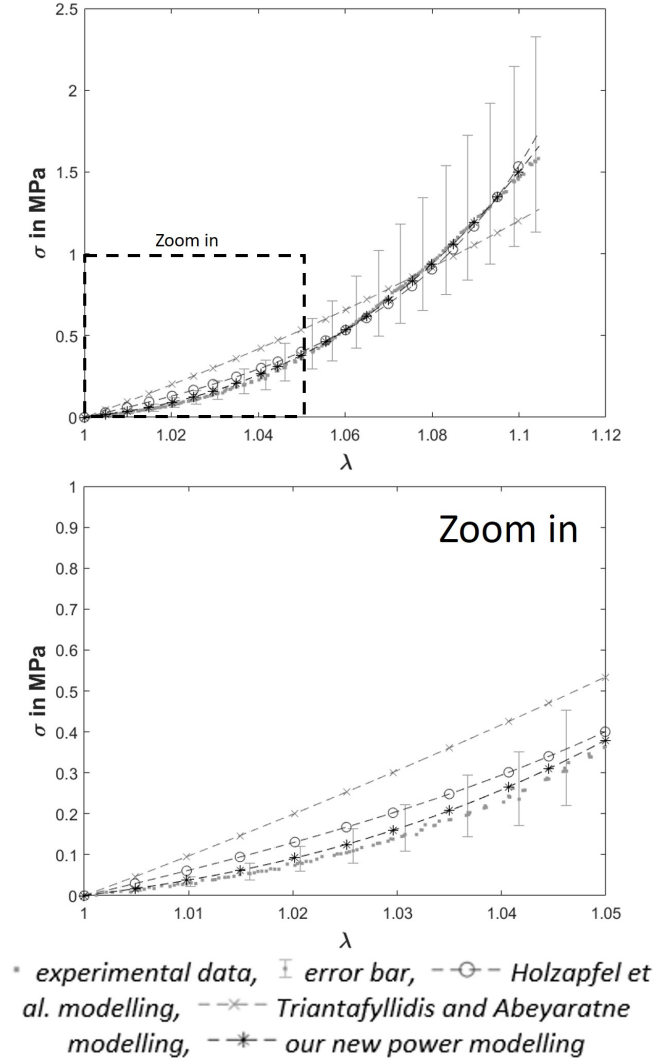
Figure 9: Comparaison of all models for specimen number 5

$$P(X \leq x) = \begin{cases} e^{-(\frac{x}{s})^{\alpha}} & \text{if } x > 0 \\ 0 & \text{else} \end{cases} \tag{14}$$

Where $\alpha > 0$ is a shape parameter and $s > 0$ a scale parameter.

As plotted in Figure 10, the Frechet law that best fits the distribution is obtained with parameters $\alpha = 1.65$ and $s = 3.99$.

The P-value relating the theoretical distribution of Frechet's law to the current distribution of Young's moduli is 0.88. Such a P-value is high, much larger than the decision threshold of 0.05 (commonly used in frequentist statistics to decide whether the probability that the law correctly represents the data is large or small; here 0.88 is a high probability) thus providing a very good representation of the Young's moduli distribution with this Frechet's law.

With such a law, the main mode is 3.00 MPa (corresponding to the peak value of the law) and 80% of the Young's moduli population is ranked between 1MPa and 10MPa with a high probability around the mode (see Figure 10).

Such a dispersion of Young's moduli can be considered as high (around one order of magnitude). However, it should be compared with the dispersion of Young's modulus values found in

Test	Triantafyllidis			Holzapfel				New model			
	C_1 (MPa)	C_2 (MPa)	Error (MPa)	C_1 (MPa)	k_1 (MPa)	k_2 (MPa)	Error (MPa)	C_1 (MPa)	b_1 (MPa)	b_2 (MPa)	Error (MPa)
1	0	1.23	0.158	0	1.75	5.39	0.051	0.751	3.00	3.13	0.018
2	0	0.569	0.028	0	1.05	1.20	0.016	0.453	0.675	2.61	0.010
3	0	0.388	0.013	0	0.710	1.52	0.008	0.377	0.446	2.72	0.005
4	0	1.38	0.016	0	2.48	13.7	0.009	1.59	3.56	3.11	0.008
5	0	1.18	0.126	0	1.50	15.9	0.042	0.554	5.88	3.29	0.016
6	0	0.668	0.147	0	0.706	12.2	0.022	0.345	5.03	3.93	0.004
7	0	5.35	0.533	0	6.72	19.4	0.224	1.59	26.6	3.14	0.096
8	0	3.18	0.284	0	3.66	36.7	0.071	1.62	40.6	3.62	0.022
9	0	0.646	0.018	0	1.05	21.5	0.005	0.657	3.64	3.39	0.003
10	0	7.30	0.741	0	11.0	4.61	0.339	3.05	14.3	2.79	0.137
11	0	1.25	0.227	0	1.27	23.2	0.050	0.260	13.5	3.69	0.008
12	0	2.80	0.136	0	4.37	14.4	0.058	1.87	8.56	2.95	0.029
13	0	2.09	0.023	0	3.41	100	0.006	2.55	301	4.45	0.008
14	0	1.52	0.105	0	2.05	25.7	0.035	0.854	8.94	3.23	0.015
15	0	1.72	0.020	0	3.09	15.1	0.011	2.00	5.16	3.18	0.009
16	0	1.31	0.086	0	2.09	6.85	0.039	0.843	2.87	2.87	0.019
17	0	1.69	0.111	0	2.72	5.30	0.051	1.05	3.31	2.82	0.023
18	0	0.964	0.040	0	1.42	28.9	0.011	0.831	7.52	3.45	0.006
19	0	4.59	0.161	0	6.20	81.4	0.043	3.78	126	3.74	0.027
20	0	1.63	0.244	0	1.96	11.3	0.095	0.426	6.41	3.19	0.037
21	0	0.813	0.018	0	1.19	114	0.005	0.848	55.4	4.07	0.005
22	0	0.930	0.055	0	1.31	24.4	0.013	0.704	6.51	3.42	0.005
23	0	0.662	0.009	0	1.15	42.2	0.005	0.811	16.1	3.96	0.005
24	0	1.04	0.132	0	1.23	19.2	0.030	0.541	8.41	3.61	0.007
25	0	0.882	0.012	0	1.62	18.1	0.010	1.05	2.33	3.11	0.010
26	0	2.56	0.053	0	4.09	49.4	0.018	2.81	63.1	3.91	0.017
27	0	0.946	0.070	0	1.30	19.9	0.018	0.642	5.77	3.38	0.006
28	0	1.06	0.108	0	1.34	19.5	0.029	0.523	6.40	3.35	0.007

Table 2: Material parameters estimated for each fit of the 28 stretch/stress curves

the literature on other human soft tissues. This can be done, for example, thanks to the synthesis work carried out by Gefen and Dilmoney (2007). For leg muscle fascia (to our knowledge, no estimations were provided for pectoral fascia), the Young's modulus values vary between 100 MPa and 2000 MPa. For fat tissue, the data varies between 0.5 kPa and 25 kPa. For the gland, the moduli range from 7.5 kPa to 66 kPa. Finally, the values provided for knee ligaments (taken as a reference for Cooper's ligaments in the Gefen and Dilmoney (2007) study) vary between 80 MPa and 400 MPa. These values show, therefore, similar, or even larger, dispersions as the ones measured for Cooper's ligaments. Stiffening can be seen by the slope of the curve at the largest

strains, for example at 5%, or by the evolution of the parameters of the hyperelastic constitutive equation. The stiffening of the material is characterised by the increase of the tangent modulus with the strain. To evaluate the stiffening, the tangent modulus at 5% can be analysed (5% is large enough to reach the hardening and few enough to reach the breaking point).

There is a large dispersion of the parameters describing the anisotropic power law. This is due to the significant differences in the experimental results obtained. It can be seen that there can be a ratio of more than 10 on the stress levels for a given strain. This result generates large variations in the parameters of the constitutive equation, due to the curvature of the

Test	Young's Modulus (MPa)	Tangent Modulus (MPa)
1	4.51	11.2
2	2.72	6.05
3	2.26	4.20
4	9.54	14.9
5	3.32	14.8
6	2.07	5.19
7	9.54	78.3
8	9.72	53.6
9	3.94	8.98
10	18.3	74.9
11	1.56	15.1
12	11.2	36.6
13	15.3	NaN
14	5.12	23.4
15	12.0	18.6
16	5.06	15.7
17	6.30	18.3
18	4.99	15.0
19	22.7	NaN
20	2.56	17.0
21	5.09	NaN
22	4.22	13.8
23	4.87	NaN
24	3.25	12.5
25	6.30	NaN
26	16.9	NaN
27	3.85	13.0
28	3.14	14.2

Table 3: Young's modulus deduced form C_1 (New modelling) and Tangent modulus (at a strain of 5%) for each tests

experimental results. Depending on the curvature of the stiffening, it can be more described by the multiplicative parameter b_1 or the power parameter b_2, so there is a compensation between the two parameters, which is the limit of the model with respect to the experimental dispersion at the stiffening.

4 Conclusion

For the first time in the literature, this paper has characterised the behaviour of breast Cooper's ligaments through uniaxial tensile tests. A new anisotropic, hyperelastic constitutive model had to be introduced in order to fit the experimental stretch/stress curves measured on 28 specimens in this particular case where data is limited.

By looking at the curves for small strains, it was interesting to estimate an order of magnitude of the Young's modulus ($E = 6C_1$ (11) for our proposed constitutive model) for each specimen, despite the dispersion observed. Our results show a distribution of the Young's modulus values that ranges between 1 MPa and 10 MPa, with a mode at 3.00 MPa.
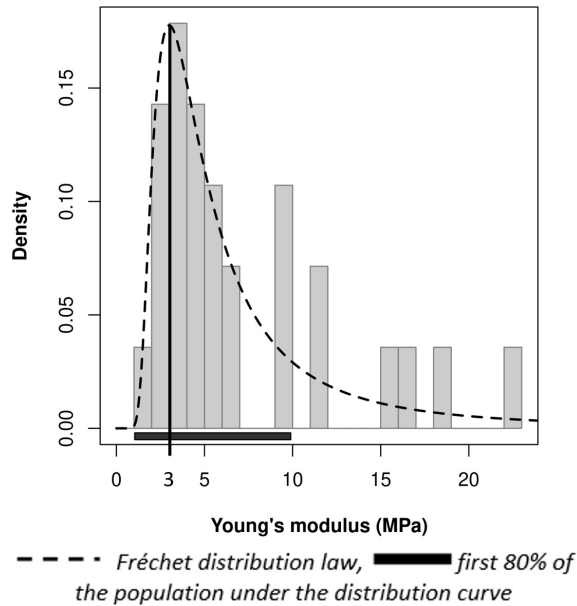
Figure 10: Histogram representing the distribution density of the 28-Young's moduli obtained from tests

Such results are very different from the Young's modulus values of the Cooper's ligaments which can be found in Gefen and Dilmoney (2007) and that vary between 80 MPa and 400 MPa. However, these values are questionable since they have been deduced from other collagenous tissues such as the knee ligaments. It is also interesting to note that the 1 MPa – 10 MPa ranging values obtained from our work show that Cooper's ligaments are two to three order of magnitude stiffer than the other constituents of breast tissue (fat, gland and muscle).

Finally, we must acknowledge that our results were obtained from a single cadaver, namely the body of a 100-year-old embalmed woman. This is a strong limitation and our conclusion will have to be verified with a much larger cohort of bodies, including fresh cadavers. Nevertheless, the results of the analysis are not disturbed by variations from one individual to another. And it remains, to our knowledge, the first study with quantitative proposals for the constitutive behaviour of Cooper's ligaments that can be now used in Finite Element models of the human breast (Mîra et al., 2018).

5   Acknowledgements

References

Azar, F. S., Metaxas, D. N., and Schnall, M. D. (2000). A finite element model of the breast for predicting mechanical deformations during biopsy procedures. In *Proceedings IEEE Workshop on Mathematical Methods in Biomedical Image Analysis. MMBIA-2000 (Cat. No. PR00737)*, pages 38–45. IEEE.

Azar, F. S., Metaxas, D. N., and Schnall, M. D. (2001). A deformable finite element model of the breast for predicting mechanical deformations under external perturbations. *Academic Radiology*, 8(10):965–975.

Briot, N., Chagnon, G., Masri, C., Girard, E., and Payan, Y. (2020). Ex-vivo mechanical characterisation of the breast cooper's ligaments. *Computer Methods in Biomechanics and Biomedical Engineering. Proceedings of the 25th Conference of the French Biomechanics Society, Metz, France.*, 23(sup1):S49–S51.

Canene-Adams, K. (2013). Preparation of formalin-fixed paraffin-embedded tissue for immuno-histochemistry. *Methods in enzymology*, 533:225–233.

Carter, T. J. (2009). *Biomechanical modelling of the breast for image-guided surgery.* PhD thesis, University of London.

Chagnon, G., Rebouah, M., and Favier, D. (2015). Hyperelastic energy densities for soft biological tissues: a review. *Journal of Elasticity*, 120(2):129–160.

Chung, J.-H., Rajagopal, V., Nielsen, P. M., and Nash, M. P. (2008). Modelling mammographic compression of the breast. In *International Conference on Medical Image Computing and Computer-Assisted Intervention*, pages 758–765. Springer.

Del Palomar, A. P., Calvo, B., Herrero, J., López, J., and Doblaré, M. (2008). A finite element model to accurately predict real deformations of the breast. *Medical engineering & physics*, 30(9):1089–1097.

Gaskin, K. M., Peoples, G. E., and McGhee, D. E. (2020). The fibro-adipose structure of the female breast: A dissection study. *Clinical Anatomy*, 33(1):146–155.

Gefen, A. and Dilmoney, B. (2007). Mechanics of the normal woman's breast. *Technology and Health Care*, 15(4):259–271.

Han, L., Hipwell, J. H., Tanner, C., Taylor, Z., Mertzanidou, T., Cardoso, J., Ourselin, S., and Hawkes, D. J. (2011). Development of patient-specific biomechanical models for predicting large breast deformation. *Physics in Medicine & Biology*, 57(2):455.

Holzapfel, G. A., Gasser, T. C., and Ogden, R. W. (2000). A new constitutive framework for arterial wall mechanics and a comparative study of material models. *Journal of elasticity and the physical science of solids*, 61(1-3):1–48.

Jemioło, S. and Telega, J. (2001). Transversely isotropic materials undergoing large deformations and application to modelling of soft tissues. *Mechanics Research Communications*, 28(4):397–404.

Lapuebla-Ferri, A., del Palomar, A. P., Herrero, J., and Jiménez-Mocholí, A.-J. (2011). A patient-specific fe-based methodology to simulate prosthesis insertion during an augmentation mammoplasty. *Medical engineering & physics*, 33(9):1094–1102.

Laurent, C. (2018). Micromechanics of ligaments and tendons. In *Multiscale Biomechanics*, pages 489–509. Elsevier.

Masri, C., Chagnon, G., and Favier, D. (2017). Influence of processing parameters on the macroscopic mechanical behavior of pva hydrogels. *Materials Science and Engineering: C*, 75:769–776.

Mîra, A., Carton, A.-K., Muller, S., and Payan, Y. (2018). A biomechanical breast model evaluated with respect to mri data collected in three different positions. *Clinical Biomechanics*, 60:191–199.

Ruiter, N. V., Stotzka, R., Muller, T.-O., Gemmeke, H., Reichenbach, J. R., and Kaiser, W. A. (2006). Model-based registration of x-ray mammograms and mr images of the female breast. *IEEE Transactions on Nuclear Science*, 53(1):204–211.

Samani, A., Bishop, J., Yaffe, M. J., and Plewes, D. B. (2001). Biomechanical 3-d finite element modeling of the human breast using mri data. *IEEE transactions on medical imaging*, 20(4):271–279.

Samani, A., Zubovits, J., and Plewes, D. (2007). Elastic moduli of normal and pathological human breast tissues: an inversion-technique-based investigation of 169 samples. *Physics in medicine & biology*, 52(6):1565.

Treloar, L. (1943). The elasticity of a network of long-chain molecules—ii. *Transactions of the Faraday Society*, 39:241–246.

Triantafyllidis, N. and Abeyaratne, R. (1983). Instabilities of a finitely deformed fiber-reinforced elastic material.

Appendix - Calculation of the initial modulus

An uniaxial tension in $\vec{e_1}$ direction with fibres oriented along $\vec{e_1}$ is considered.

1 General equations

Stress-Strain relation for a hyperelastic energy density depending of I_1 and I_4 is defined as in a general way and can be written in uniaxial extension:

$$\bar{\bar{\sigma}} = -p\bar{\bar{I}} + 2\frac{\partial W}{\partial I_1}\bar{\bar{B}} + 2\frac{\partial W}{\partial I_4}\bar{\bar{F}}\vec{a_0} \otimes \vec{a_0}\bar{\bar{F}}^T$$

$$\begin{bmatrix} \sigma & 0 & 0 \\ 0 & 0 & 0 \\ 0 & 0 & 0 \end{bmatrix} = -p\begin{bmatrix} 1 & 0 & 0 \\ 0 & 1 & 0 \\ 0 & 0 & 1 \end{bmatrix} + 2\frac{\partial W}{\partial I_1}\begin{bmatrix} \lambda^2 & 0 & 0 \\ 0 & \frac{1}{\lambda} & 0 \\ 0 & 0 & \frac{1}{\lambda} \end{bmatrix} + 2\frac{\partial W}{\partial I_4}\begin{bmatrix} \lambda^2 & 0 & 0 \\ 0 & 0 & 0 \\ 0 & 0 & 0 \end{bmatrix} \tag{1}$$

Let's consider $\lambda = 1 + \varepsilon$ where ε is the nominal strain. In the following, ε is considered small for linearisation.

2 Neo-Hookean and Triantafillidis model

$$W = C_1(I_1 - 3) + C_2(I_4 - 1)^2$$

$$\frac{\partial W}{\partial I_1} = C_1$$

$$\frac{\partial W}{\partial I_4} = 2C_2(I_4 - 1)$$

$$\sigma = -\frac{2C_1}{1+\varepsilon} + 2C_1(1+\varepsilon)^2 + 4C_2\left((1+\varepsilon)^2 - 1\right)(1+\varepsilon)^2$$

$$\sigma = (6C_1 + 8C_2)\varepsilon + o(\varepsilon)$$

$$E = 6C_1 + 8C_2$$

The Young Modulus can be identified by $6C_1 + 8C_2$.

3 Neo-Hookean and Holzapfel model

$$W = C_1(I_1 - 3) + \frac{k_1}{2k_2}\left(e^{k_2(I_4 - 1)^2} - 1\right)$$

$$\frac{\partial W}{\partial I_1} = C_1$$

$$\frac{\partial W}{\partial I_4} = k_1(I_4 - 1)e^{k_2(I_4 - 1)^2}$$

$$\sigma = -\frac{2C_1}{1+\varepsilon} + 2C_1(1+\varepsilon)^2 + 2\left(k_1\left((1+\varepsilon)^2 - 1\right)e^{k_2\left((1+\varepsilon)^2 - 1\right)^2}\right)(1+\varepsilon)^2$$

$$\sigma = (6C_1 + 4k_1)\varepsilon + o(\varepsilon)$$

$$E = 6C_1 + 4k_1$$

The Young Modulus can be identified by $6C_1 + 4k_1$.

4 Neo-Hookean and New Model

$$W = C_1(I_1 - 3) + b_1(I_4 - 1)^{b_2}$$

$$\frac{\partial W}{\partial I_1} = C_1$$

$$\frac{\partial W}{\partial I_4} = b_1 b_2 (I_4 - 1)^{b_2 - 1}$$

$$\sigma = -\frac{2C_1}{1 + \varepsilon} + 2C_1(1 + \varepsilon)^2 + 2b_1 b_2 \left((1 + \varepsilon)^2 - 1\right)^{b_2 - 1} (1 + \varepsilon)^2$$

$$\sigma = -2C_1 \left(1 - \varepsilon + o(\varepsilon)\right) + 2C_1 \left(1 + 2\varepsilon + o(\varepsilon)\right) + 2b_1 b_2 \left(2\varepsilon + \varepsilon^2\right)^{b_2 - 1} (1 + 2\varepsilon + o(\varepsilon))$$

$$\sigma = 6C_1\varepsilon + 2b_1 b_2 (2\varepsilon)^{b_2 - 1} (1 + 2\varepsilon) + o(\varepsilon)$$

(4)

For $b_2 = 2$:

$$\sigma = 6C_1\varepsilon + 8b_1\varepsilon (1 + 2\varepsilon) + o(\varepsilon)$$

$$\sigma = (6C_1 + 8b_1)\varepsilon + o(\varepsilon)$$

$$E = 6C_1 + 8b_1$$

(5)

The Young Modulus can be identified by $6C_1 + 8b_1$.

For $b_2 > 2$:

$$\sigma = 6C_1\varepsilon + 2b_1 b_2 (2\varepsilon)^{b_2 - 1} (1 + 2\varepsilon) + o(\varepsilon)$$

$$\sigma = 6C_1\varepsilon + o(\varepsilon)$$

$$E = 6C_1$$

(6)

The Young Modulus can be identified by $6C_1$.